Influence of Bolted-Joint Slippage on the Response of Transmission Towers Subjected to Frost-Heave

by

K.I.E. Ahmed, R.K.N.D. Rajapakse and M.S. Gadala

Reprinted from

Advances in Structural Engineering

Volume 12 No. 1 2009

MULTI-SCIENCE PUBLISHING CO. LTD.
5 Wates Way, Brentwood, Essex CM15 9TB, United Kingdom

Influence of Bolted-Joint Slippage on the Response of Transmission Towers Subjected to Frost-Heave

K.I.E. Ahmed, R.K.N.D. Rajapakse* and M.S. Gadala

Department of Mechanical Engineering, The University of British Columbia, Vancouver, Canada V6T 1Z4

Abstract: Slippage of bolted joints is an important factor in the behavior of transmission towers. Field inspections of towers located in the northern regions of Canada show substantial frost-heave induced displacements. The conventional structural analysis software solutions for tower leg axial forces, based on idealized joint behavior under field-observed frost-heave induced displacements, are excessively large, implying tower failure in some cases. However, field inspections show structurally stable towers, and design engineers often consider joint slippage as the main reason for this discrepancy. In this paper, the experimental slippage behavior of transmission-tower bolted joints investigated by Ungkurupanian (2000) is incorporated into a non-linear joint finite element and applied to study the behavior of transmission towers under working loads by using the finite element method. The analysis shows that tower-leg joint slippage has a significant influence on tower behavior by either reducing the load carrying capacity or significantly increasing the deflections under working loads. On the other hand, joint slippage has a positive effect on towers subjected to frost-heave induced displacements, as the resulting member axial forces are much lower than those corresponding to rigid joints.

Key words: bolted joints, finite element method, frost-heave, slippage, structural analysis, transmission towers.

1. INTRODUCTION

Transmission towers are mostly latticed steel structures, and their structural integrity is a key factor in the reliability of a power transmission system. A latticed transmission tower consists of steel columns made out of angled sections, which are the main legs, and horizontal and diagonal bracings connected to the legs to provide lateral stability. The primary tower design loads are related to the self-weight of the conductor wires and tower members, and environmental loads such as wind, earthquake and ice loads.

In cold regions such as the northern parts of Canada, frost-heave is an important factor in tower behaviour. Structural engineers from electric power utilities have long recognized the need for better understanding of the response of towers subjected to frost-heave. Site inspections in northern Manitoba have shown differential displacements amounting to over 300mm at the tower leg bases. Conventional structural analysis software commonly used by engineers for latticed-tower analysis is based on the assumption of either pin-ended trusses or 3-D frames with rigid joints. Design engineers find that tower leg members are subjected to loads exceeding their ultimate design loads when a tower is analyzed using standard structural analysis software under typical frost-heave induced displacements. However, site inspections show that the towers are stable and structurally sound.

A possible explanation for the discrepancy between the member forces predicted by standard software and actual tower forces is the idealized joint behavior (pinned or rigid joints) assumed in the analysis. Transmission tower joints are bolted joints, which are in

*Corresponding author. Email address: rajapakse@mech.ubc.ca; Fax: +604-822-9013; Tel: +604-827-4483.

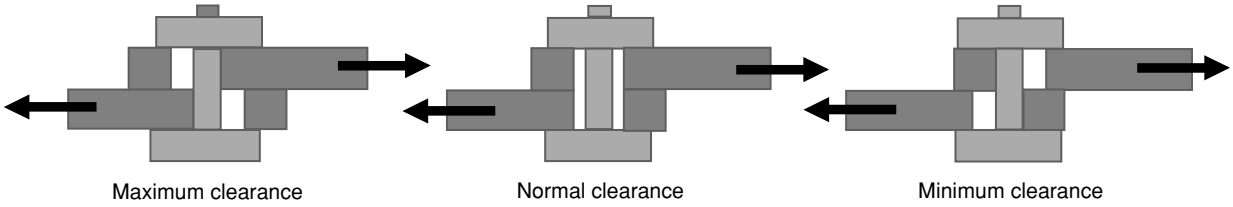

Figure 1. Different clearance configurations of a bolted joint

reality neither pinned nor rigid joints. The importance of joint slippage in connection with transmission towers was first noticed by structural engineers who observed, during full-scale tests, that the actual lateral deformation of a tower is much larger than the deflection derived through structural analysis. Tower design engineers believe that bolted joints allow for significant slippage at the joints and thereby allow substantial redistribution of member forces when towers are subjected to frost-heave. It is therefore useful to examine the behavior of towers under frost-heave by a refined structural analysis that accounts for joint slippage and other important characteristics. Findings of such a study would be useful to power utilities to improve the current design and construction practices for towers subjected to frost-heave. In addition, tower maintenance practices would benefit from a better understanding of the tower member forces and deformations due to frost-heave, as most towers subjected to frost-heave are located in remote regions with limited access for maintenance.

Many studies have examined the behavior of bolted joints under different loading conditions. A simple bolted joint consists of two members and a bolt. The diameter of the hole in each member is slightly larger than the bolt diameter, leaving some clearance between the bolt and members. A bolted joint has three configurations, as shown in Figure 1: minimum clearance, normal clearance, and maximum clearance. Due to the clearance between the hole and the bolt, the two members start to slip over each other after reaching the threshold slippage load. The stiffness of the joint before slippage is lower than that of the member, however, with similar linear behavior. After slippage starts, the joint stiffness reduces dramatically until the joint reaches a bearing stage. The stiffness then starts to increase slightly until it reaches the yielding point. The maximum, normal, and minimum clearance arrangements reach the same yielding point.

Several researchers have presented analytical models that consider non-perfect joint behavior. Chen and Lui (1987) modified a beam-column joint to include a flexible connection spring. Al-Bermani and Kitipornchai (1992) extended this procedure to a three-dimensional beam-column element. Peterson (1962) concluded that up to one-half of the measured deflections of transmission towers could be due to bolt slippage, with the remainder due to elastic deformation. Marjerrison (1968) concluded that the deformations of holes and bolts of tower joints are responsible for increasing the theoretical deflections of a tower by three times. Bolt slippage in towers was first simulated by Williams and Brightwell (1987). Devlecchio and Soom (1991) studied the effect of statistical tolerances of location on the amount of available slippage or movement that can occur in bolted assemblies.

Kitipornchai *et al.* (1994) developed two idealized slippage models, namely instantaneous and continuous slippage models, to study the effect of bolt slippage on the ultimate strength and deformations of transmission towers. They concluded that bolt slippage has no effect on tower load-carrying capacity but significantly affects the deformation of a tower under working loads. Kroeker (2000) analyzed a full-scale transmission tower with joint slippage using the continuous slippage model of Kitipornchai *et al.* (1994). In Ungkurapinan (2000) and Ungkurapinan *et al.* (2003), an extensive experimental study on the stiffness of three types of joints commonly used in transmission towers is reported.

Current commercial structural analysis software requires further improvements to account for joint slippage when applied to analysis of transmission towers. Joint-slippage modeling should be based on reliable experimental data. The recent study by Ungkurapinan (2000) provides a sound experimental basis for analyzing the behavior of bolted joints in transmission towers, incorporating joint slippage, as well as bending and geometric stiffness of leg members. The experimental data obtained by Ungkurapinan (2000) are analyzed for two joint types; column-to-column and beam-to-column, to obtain equivalent joint parameters such as joint stiffness, yield strength, etc. The experimentally observed joint behavior is incorporated into a finite element model. The response of selected tower structures under frost-heave induced displacements is examined to understand the influence of joint slippage on towers subjected to frost-heave.

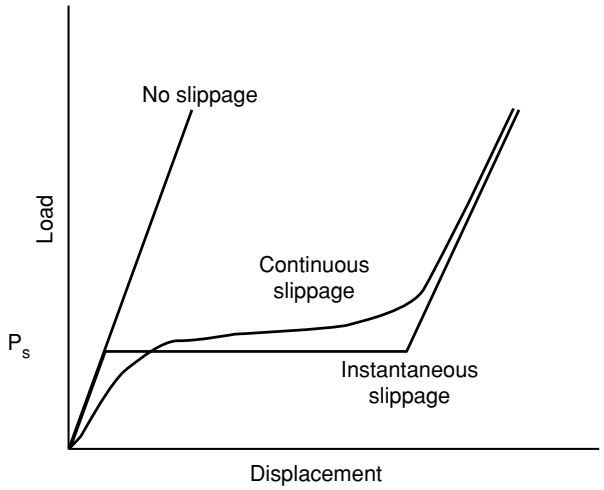

Figure 2. Instantaneous and continuous slippage models

2. BOLTED JOINT BEHAVIOR

The numerical simulation of bolted joints has been carried out based on either instantaneous or continuous slippage models (Kitipornchai *et al*. 1994).

In the instantaneous slippage model, a joint is assumed to start slipping at an axial load, P_s. The joint continues to slip while P_s is constant until the joint clearance is fully reached (Figure 2). The final amount of slippage Δ_s is added to the element length L in the case of tension members and subtracted from the member length for compression members. The joint behavior represented by this model does not favorably match the experimental results reported by Ungkurapinan (2000). In the continuous slippage model, it is assumed that slippage takes place continuously and can be represented by a Ramberg-Osgood type function. The model behavior is highly sensitive to the values of the exponents of the Ramberg-Osgood function, which affects the shape of the load-deformation relation.

The above two models do not take into account the yielding of a joint, which depends on material and joint types (Ungkurapinan 2000). The experimental findings of Ungkurupinan (2000) show that different bolted joints have different stiffness characteristics and slippage behavior. In addition, slippage of a particular joint type depends on the arrangement of bolts and bolt clearances.

In order to account for joint slippage in towers in a more complete manner, the present study aims to develop joint finite elements based on the experimental work done by Ungkurapinan (2000), who obtained the axial stiffness of a series of bolted joints through an experimental program. After reviewing of different types of joints in transmission towers used by Manitoba Hydro, Ungkurapinan (2000) identified three representative joint types to describe the tower joint behaviour, and conducted a comprehensive experimental investigation. The first type of joint is the tower leg-splice joint, labeled by Ungkurupinan (2000) as "Series A joints"; the second type is the web-bracing member joint connecting diagonal bracings to horizontal bracings, labeled as "Series B joints"; and the third type is the joint representing splice connection of a leg in the top part of a tower or a long diagonal bracing, labeled as "Series C joints." Each joint type was tested with three different clearance configurations: maximum, normal, and minimum. For Type-A joints, Ungkurapinan (2000) measured the deformations at the joint ends and at each of the bolts to examine the joint behavior under compression loading. Since the current study focuses on joint stiffness, only the deformations at the joint ends are considered. Figure 3 shows the measured behavior of the three configurations of Type-A joints under loading.

For Type-C joints, Ungkurapinan (2000) measured the deformations at the joint ends and at each of the bolts to determine the contribution of each bolt to joint behavior. Type-C joints with one, two, three, and four bolts were tested by Ungkurapinan (2000) for the three clearance configurations. Figure 4 shows the typical behavior of the three configurations of Type-C joints obtained from these experiments for joints with one or two bolts.

3. FINITE ELEMENT MODELING

3.1. 3-D Beam and Truss Elements

In the current work, the tower leg joints are assumed to slip and are represented by Type-A joints, whereas all bracing member joints are assumed to be Type-C joints for simplicity. However, the analysis presented in this section places no restriction on adding other types of joints such as Type-B joints, provided the appropriate experimental results for joint behaviour are available. Transmission tower leg members are generally subjected to bending loads in addition to significant axial loads, both of which are modeled in this study using 3-D beam elements. Members carrying primarily axial forces such as diagonal bracings are modeled as truss elements. Horizontal bracings are modeled as beam elements to account for both axial and bending loads. In the following finite element analysis, the geometric stiffness due to member axial load is considered but strains are assumed to be infinitesimal. Material non-linearity is not considered, as only the working-load response of towers is examined.

Figure 5 shows a three-dimensional beam finite element with the local coordinate axes, *x, y* and *z*; global coordinate axes, *X*, *Y* and *Z*, and the local and global

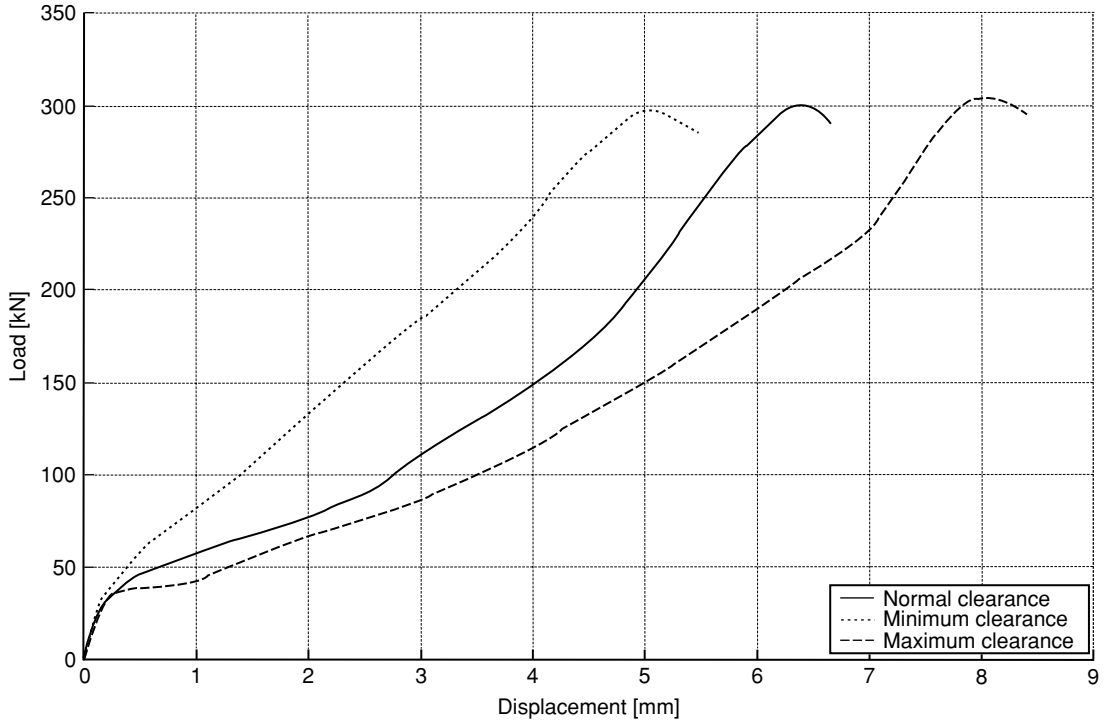

Figure 3. Typical test results for the three configurations of Type-A joints as reported by Ungkurapinan (2000)

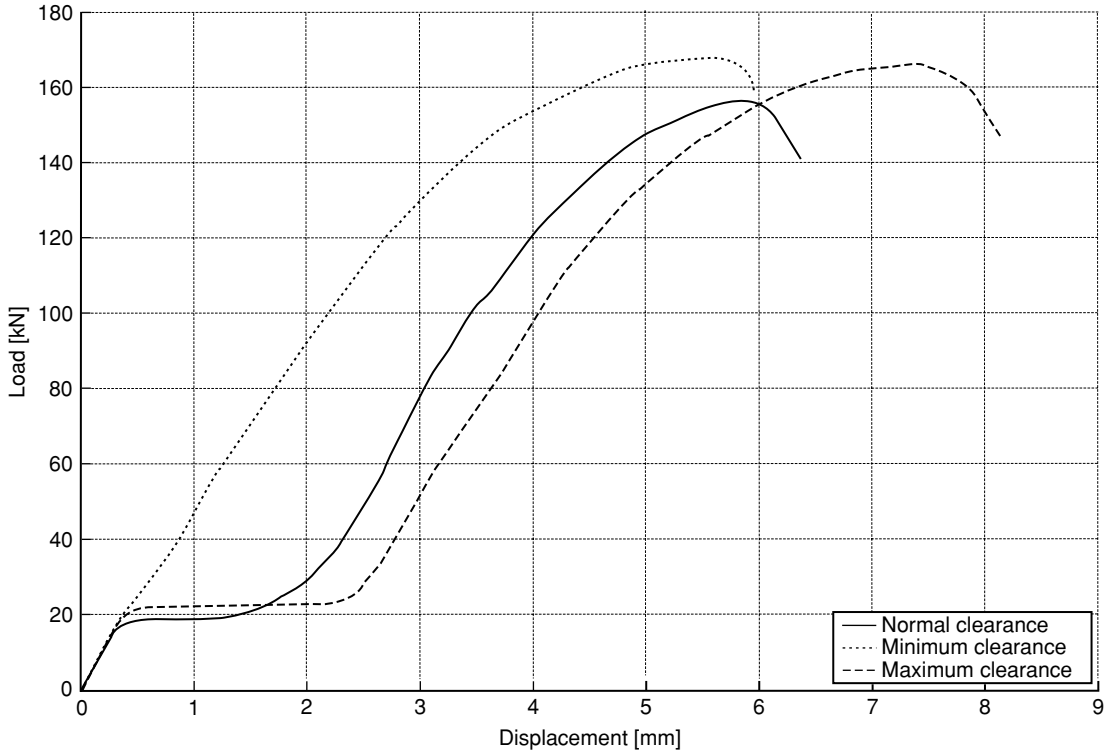

Figure 4. Typical test results for the three configurations of Type-C joints as reported by Ungkurapinan (2000)

degrees of freedom (DOF) at the nodes '*i*' and '*j*'. For the node *i*, the degrees of freedom in the local coordinates are denoted by u_{xi}, v_{yi}, w_{zi}, θ_{xi} , θ_{yi} , and θ_{zi} whereas the degrees of freedom in the global coordinates are denoted by u_{Xi} , u_{Yi} , u_{Zi} , θ_{Xi} , θ_{Yi} , θ_{Zi}. The beam element shown in Figure 5 can be subjected to bending deformations in the *xy* and *xz* planes. The stiffness matrix in the local coordinates can be found in a standard structural engineering textbook (Ghali and Neville 1987).

The geometric stiffness matrix in the local coordinates is given (Przemieniecki 1968) by:

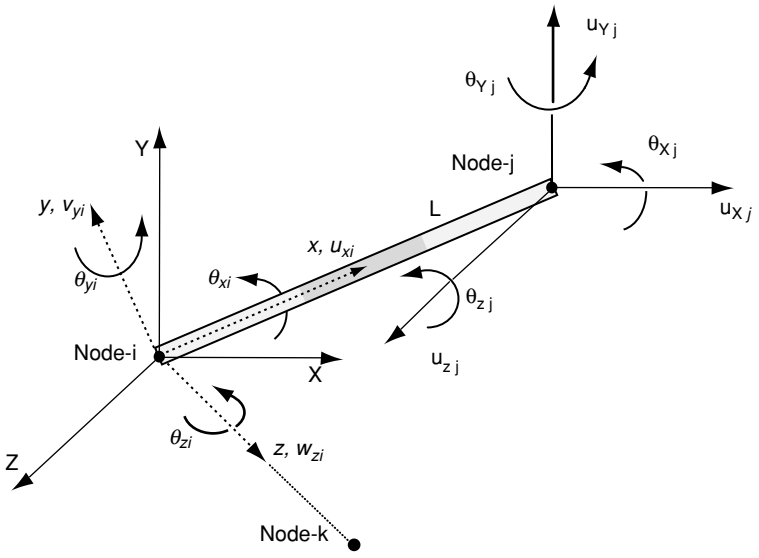

Figure 5. Three-dimensional beam element and degrees of freedom

$$\left[\mathbf{K}^{(\sigma)}\right]_{xyz}=\frac{P}{30L}\begin{bmatrix}0 & 0 & 0 & 0 & 0 & 0 & 0 & 0 & 0 & 0 & 0 & 0\\ & 36 & 0 & 0 & 0 & 3L & 0 & -36 & 0 & 0 & 0 & 3L\\ & & 36 & 0 & -3L & 0 & 0 & 0 & -36 & 0 & -3L & 0\\ & & & 0 & 0 & 0 & 0 & 0 & 0 & 0 & 0 & 0\\ & & & & 4L^2 & 0 & 0 & 0 & -3L & 0 & -L^2 & 0\\ & & & & & 4L^2 & 0 & 3L & 0 & 0 & 0 & -L^2\\ & & & & & & 0 & 0 & 0 & 0 & 0 & 0\\ & & & \text{Symm} & & & & 36 & 0 & 0 & 0 & -3L\\ & & & & & & & & 36 & 0 & 3L & 0\\ & & & & & & & & & 0 & 0 & 0\\ & & & & & & & & & & 4L^2 & 0\\ & & & & & & & & & & & 4L^2\end{bmatrix} \quad (1)$$

where L and P denote the member length and axial force, respectively.

The nodal DOF and force vectors corresponding to Eqn 1 are defined as,

$$\begin{aligned}\{u\}_{xyz}&=\left[u_{ix}\ \ u_{iy}\ \ u_{iz}\ \ \theta_{ix}\ \ \theta_{iy}\ \ \theta_{iz}\ \ u_{jx}\ \ u_{jy}\ \ u_{jz}\ \ \theta_{jx}\ \ \theta_{jy}\ \ \theta_{jz}\right]^T,\\ \{F\}_{xyz}&=\left[F_{ix}\ \ F_{iy}\ \ F_{iz}\ \ M_{ix}\ \ M_{iy}\ \ M_{iz}\ \ F_{jx}\ \ F_{jy}\ \ F_{jz}\ \ M_{jx}\ \ M_{jy}\ \ M_{jz}\right]^T\end{aligned} \quad (2)$$

where M_x, M_y, and M_z are the bending moments about the x-axis, y-axis, and z-axis, respectivel, F_x, F_y, and F_z are the forces in the directions of x-axis, y-axis, and z-axis, respectively.

The total stiffness matrix is the sum of the linear and stress stiffness matrices:

$$\left[\mathbf{K}\right]_{xyz}=\left[\mathbf{K}^{(t,b)}\right]_{xyz}+\left[\mathbf{K}^{(\sigma)}\right]_{xyz} \quad (3)$$

The stiffness matrix in the global coordinates (Zienkewicz and Taylor 1989) is given by,

$$\left[K\right]_{XYZ}=\left[T\right]^T\left[K\right]_{xyz}\left[T\right] \quad (4)$$

where $[K]_{XYZ}$ is the stiffness matrix in the global coordinates and $[T]$ is the element coordinate transformation matrix.

The elements of the coordinate transformation matrix are calculated from the nodal coordinates of an element, and [T] have to be updated based on the current position coordinates and definition of the centroidal principal local axes of the beam cross-section. For 3-D beam elements, the two nodal coordinates of an element cannot uniquely define the orientation of its local coordinates. Thus, an extra node k, located on the local x- and z- axes (Figure 5), is required. This node defines an orientation angle, β, of the element local y-axis to the global X-Y plane. Thus, for an element with the nodal coordinates (x_i, y_i, z_i) and (x_j, y_j, z_j), a third node with coordinates (x_k, y_k, z_k) defines the angle (β) according to the following relation (ANSYS Manual 2005).

$$\begin{aligned}\cos(\beta)&=\frac{(\mathbf{V_1}\times\mathbf{e})\cdot(\mathbf{V_1}\times\mathbf{V_2})}{|(\mathbf{V_1}\times\mathbf{e})|\cdot|(\mathbf{V_1}\times\mathbf{V_2})|}\quad \textit{and}\\ \sin(\beta)&=\frac{\mathbf{V_1}\cdot((\mathbf{V_1}\times\mathbf{e})\times(\mathbf{V_1}\times\mathbf{V_2}))}{|(\mathbf{V_1})|\cdot|(\mathbf{V_1}\times\mathbf{e})|\cdot|(\mathbf{V_1}\times\mathbf{V_2})|}\end{aligned} \quad (5)$$

where

$\mathbf{V_1}$ is a vector along the element x-axis between nodes i and j

$\mathbf{V_2}$ is a vector in the element x-z plane between nodes i and k

e is a unit vector parallel to the global Z-axis, unless $\mathbf{V}_1$ is parallel to the Z-axis, in which case "**e**" is taken to be parallel to the X-axis.

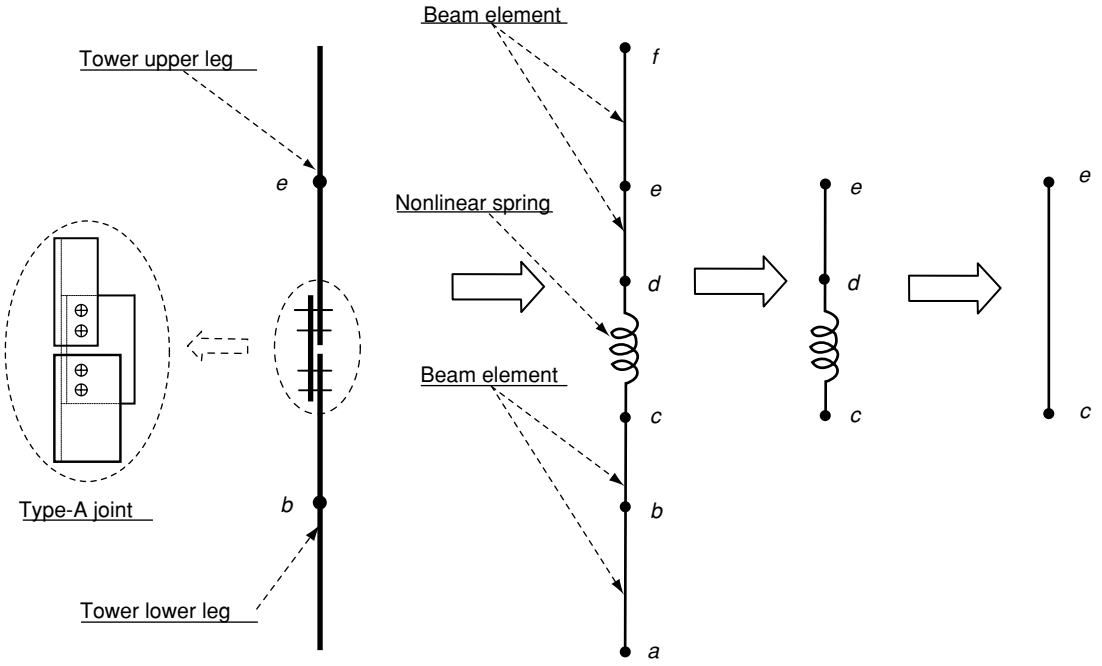

Figure 6. A Type-A joint and finite element model

With this definition of β, it can be shown that

$$[T]=\begin{bmatrix} \frac{\Delta x}{L} & \frac{\Delta y}{L} & \frac{\Delta z}{L} \\ \frac{(\Delta x)(\Delta z)(S/L)-(\Delta y)C}{\sqrt{(\Delta x)^2+(\Delta y)^2}} & \frac{(\Delta x)C-(\Delta y)(\Delta z)(S/L)}{\sqrt{(\Delta x)^2+(\Delta y)^2}} & \frac{LS}{\sqrt{(\Delta x)^2+(\Delta y)^2}} \\ -\frac{(\Delta x)(\Delta z)(C/L)+(\Delta y)S}{\sqrt{(\Delta x)^2+(\Delta y)^2}} & -\frac{(\Delta y)(\Delta z)(C/L)+(\Delta x)S}{\sqrt{(\Delta x)^2+(\Delta y)^2}} & \frac{LC}{\sqrt{(\Delta x)^2+(\Delta y)^2}} \end{bmatrix} \quad (6)$$

where $C = \cos(\beta)$, $S = \sin(\beta)$ and

$$\Delta x = x_j - x_i, \qquad \Delta y = y_j - y_i, \qquad \Delta z = z_j - z_i$$

$$\textit{and} \qquad L = \sqrt{(\Delta x)^2 + (\Delta y)^2 + (\Delta z)^2}$$

The stiffness matrix of a 3-D truss element can be found in a standard text book (Ghali and Neville 1987).

3.2. Joint Modeling

3.2.1. Type-A joints

Figure 6 shows the typical configuration of a Type-A joint connecting two tower leg elements. The upper and lower tower legs are modeled by 3-D beam elements. The bolted joint connecting the two beam elements '***e-d***' and '***b-c***' is modeled as a non-linear axial spring. The joint is assumed to slip along the axial direction and behave rigidly with respect to other degrees of freedom. The non-linear spring can be lumped with the axial stiffness of the upper (or lower) beam element connected to the spring. The non-linear axial stiffness of the lumped element can be calculated as

$$K_A = K_{J_A}\left(\frac{EA}{L}\right)\Big/\left[K_{J_A}+\left(\frac{EA}{L}\right)\right] \quad (7)$$

where ***L*** is the length between nodes ("***c***" - "***e***"), ***E*** is the modulus of elasticity, ***A*** is the cross sectional area of the leg member, and K_{JA} is the axial stiffness calculated from the load-deformation curves of the Type-A joints as reported by Ungkurapinan (2000).

3.2.2. Type-C joints

The tower legs have diagonal and horizontal bracings with angle sections connected to them. The bracing elements are normally modeled as truss elements and are connected to tower legs by one, two or more bolts. These joints are modeled as Type-C joints in the present study and the joint configuration is shown in Figure 7. As in the case of Type-A joints, experimental data is available to compute joint stiffness only in the axial direction.

The joint behavior is modeled by a nonlinear axial spring similar to the case of Type-A joints. Therefore, a typical truss element has two springs at the ends, representing the joints at the ends (Figure 7). As in the Type-A joints, the joint stiffness can be lumped with the truss element axial stiffness. The equivalent axial stiffness can be calculated from Eqn 7 with the appropriate values for L, E, and A. The spring stiffness K_{JA} is replaced with "$2K_{JC}$" which is computed from the load-deformation curves of Type-C joints reported by Ungkurapinan (2000).

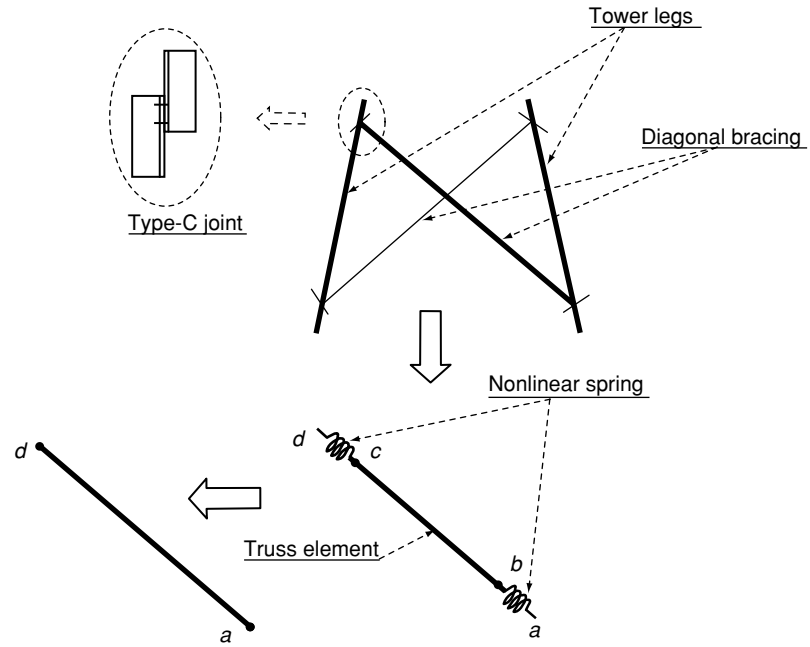

Figure 7. A Type-C joint and finite element model

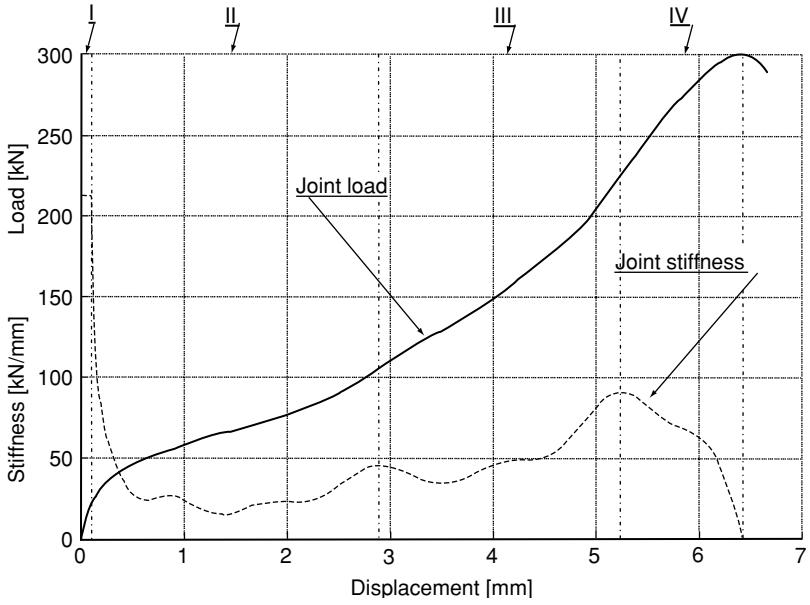

Figure 8. Different deformation regions of a bolted joint (I-micro-slipping, II-macro-slipping, III-bearing, IV-plastic zone)

3.3. Joint Stiffness Calculation

The experimentally obtained load-deformation curves of Ungkurapinan (2000) can be divided into four regions corresponding to different joint behavior mechanisms, as shown in Figure 8. The first region is the micro-slip region, in which the two connected elements are overcoming their mutual asperities. The joint stiffness in this region is much weaker than the stiffness of each element. After the asperities are shaved off, the two elements start to slip over each other, giving rise to a macro-slip region that corresponds to the lowest level of stiffness for the joint (stiffness may become singular in this region). The end of the second region is identified by the maximum clearance of the joint, and the joint response enters a third region representing a bearing state in which the load is transformed by shearing of the bolts. In the third region, the joint stiffness is slightly increased due to the addition of the bolt shear stiffness to the global stiffness. Further loading eventually gets the joint into plastic deformations when members or

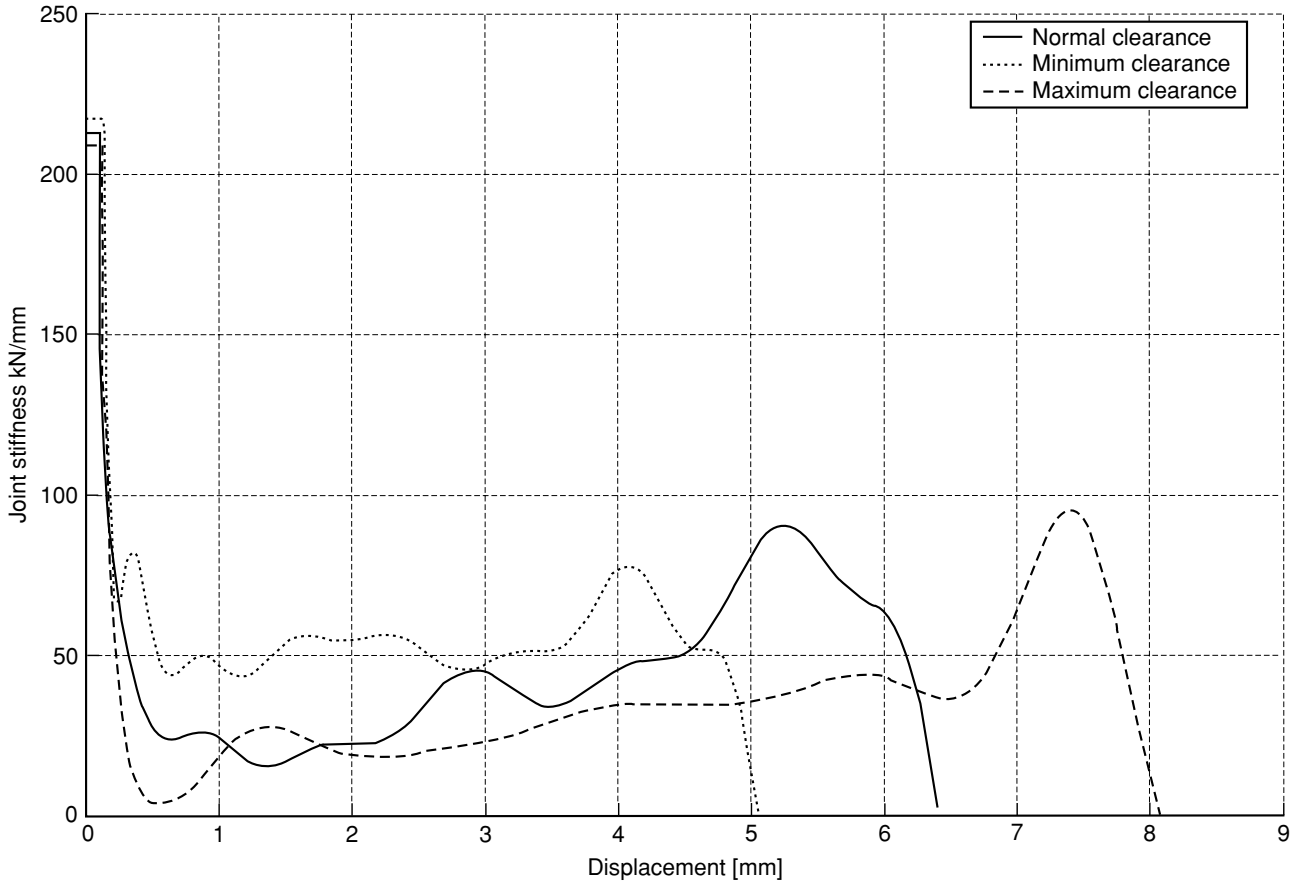

Figure 9. Computed stiffness of Type-A joints based on Ungkurupinan (2000)

bolts start to yield. Investigation of the experimental results corresponding to the fourth stage shows that yielding of the joint occurs at a load level much lower than the yield load of the connecting members. The joint load-carrying capacity is therefore much lower than that of the individual members. This important observation was not considered in the previous slippage models.

For the two types of joints discussed above, i.e., Type-A and Type-C joints, the stiffness at a given load or displacement level is obtained as the tangent to the experimental load-deflection curve at that point, i.e., $k = df/du$, by using the secant numerical differentiation technique. The finite element program developed in this study incorporates all of the experimental load-deflection curves of Ungkurupinan (2000) in a module. The second stage of continuous slippage is identified by a rapid change in the slope of the curve. The third or the onset of yielding stage is, however, not easily identifiable and the following approximation is acceptably used.

$$F_y = \frac{F_f}{S_f} \cdot S_y \tag{8}$$

where F_f is the fracture load of the joint; F_y is the yield load of the joint; S_f is the fracture stress of the member; and S_y is the yield stress of the member.

Figures 9 and 10 show the joint stiffness of the Type-A and Type-C joints calculated from the experimental results of Ungkurupinan (2000) for the three initial clearance configurations. It is worth noting that for Type-C joints the stiffness is assumed to have a very small positive value if the differentiation of the load-deformation relation gives zero or negative stiffness values. This approximation is meant to prevent a singular stiffness matrix.

3.4. Numerical Solution Scheme

For non-linear problems, the loads and specified displacements are applied incrementally and the deformed configuration has to be updated at each load increment. The finite element procedure is summarized below.

It is assumed that the solution is known at a given time t. The aim is to find the solution for time $t+\Delta t$.

1. Update the geometry; ${}^{t}\mathbf{X} = {}^{t-\Delta t}\mathbf{X} + {}^{t}\Delta\mathbf{u}$
2. Update the element dimensions;

$${}^{t}L = \sqrt{\left({}^{t}\Delta x\right)^2 + \left({}^{t}\Delta y\right)^2 + \left({}^{t}\Delta z\right)^2}$$

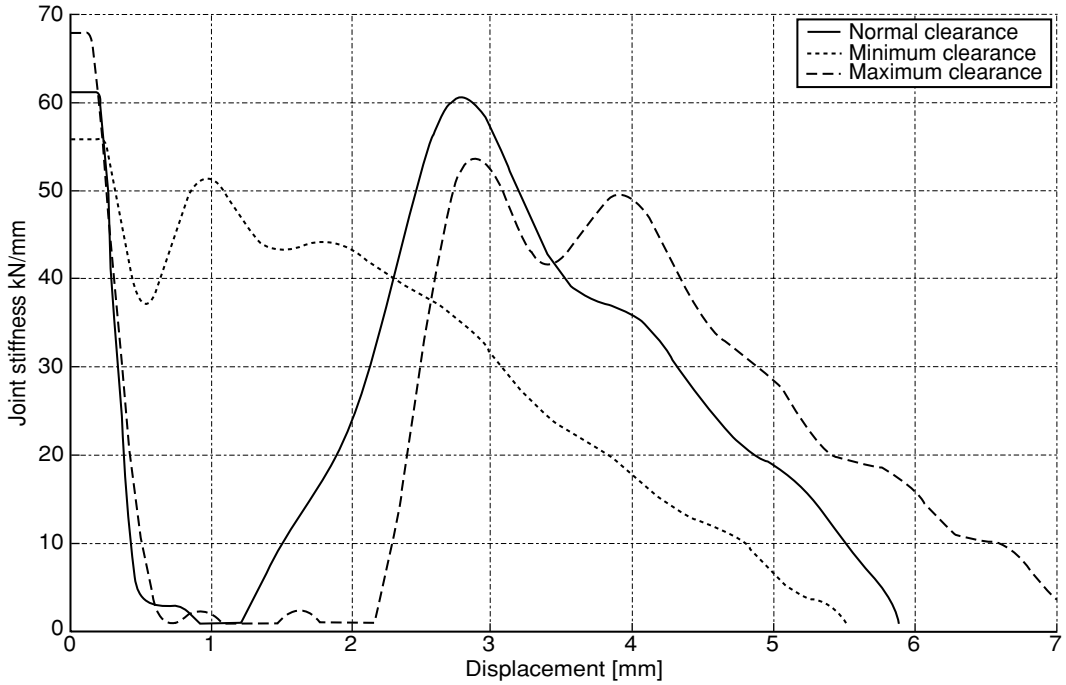

Figure 10. Computed stiffness of Type-C joints based on Ungkurupinan (2000)

3. Update the transformation matrix ${}^{t}[T] = f({}^{t}\mathbf{X})$
4. Obtain the current stiffness matrix ${}^{t}K = {}^{t}K_{linear} + {}^{t}K_{\sigma}$ using the updated geometry and loads.
5. Solve the system equation ${}^{t}K \cdot ({}^{t+\Delta t}\Delta u)_1 = {}^{t+\Delta t}\Delta F$ where ${}^{t+\Delta t}\Delta F$ is the load increment and $({}^{t+\Delta t}\Delta u)_1$ is the unknown displacement to be solved in the first iteration. The stiffness matrix in Step 4 and the displacement in Step 5 are considered as first iteration values of the load increment t+Δt
6. Update the geometry: $({}^{t+\Delta t}\mathbf{X})_i = {}^{t}\mathbf{X} + ({}^{t+\Delta t}\Delta\mathbf{u})_i$ where i is the iteration number
7. Repeat Steps 2 to 4 and solve $({}^{t+\Delta t}\mathrm{K})_i \cdot ({}^{t+\Delta t}\Delta u)_{i+1} = {}^{t+\Delta t}\Delta\mathrm{F}$ for the unknown displacements $({}^{t+dt}\Delta u)_{i+1}$ corresponding to the iteration '*i*' and continue until the convergence criterion: $({}^{t+\Delta t}\Delta u)_i - ({}^{t+\Delta t}\Delta u)_{i-1} < 1\mathrm{E}\text{-}7$ is satisfied.

4. NUMERICAL RESULTS AND DISCUSSION

4.1. 2-D Tower Structure

A finite element program based on the modeling described in the preceding sections was developed to analyze transmission tower structures. Figure 11 shows a 2-D tower structure that is analyzed to investigate the effect of joint slippage on the towers load-carrying capacity. Figure 11 also shows the finite element model with the locations and types of joints used. In all cases, the diagonal and horizontal bracing members are modeled as truss elements and the leg members as beam elements. The Type-A joints are considered at the bottom and top connection points of the tower substructure. The truss elements with Type-C joints are considered for all bracing elements. Three different models are considered: the first model with fully rigid joints, the second with one of the joint types (A or C) having slippage and the third with both types of joints having slippage. The gage size of the members is equal to the gage size of the tested joints of Ungkurupinan (2000), which is an angle section of $4 \times 4 \times 0.25$ inches.

The structure is studied under three load cases. The first load case has a lateral load that is one sixth of the vertical load (similar to Kitipornchai *et al.* 1994). In the other two load cases, the lateral load is set to one-half and one-twentieth of the vertical load. In all cases, the analyses are carried out until a maximum vertical load of 1200 N is reached or until joint yielding starts.

Selected tower-response results are shown in Figures 12 and 13. Figure 12 shows that for the first load case, when slippage of only the Type-C joints is considered, a slight reduction in the load-carrying capacity is observed compared with a structure with all fully rigid joints. Although the yield limit of a Type-C joint is very small compared to that of the column (see Table 1), the structure fails due to the yielding of the columns rather than the yielding of the Type-C joints. Figure 12 also shows that when only slippage of the

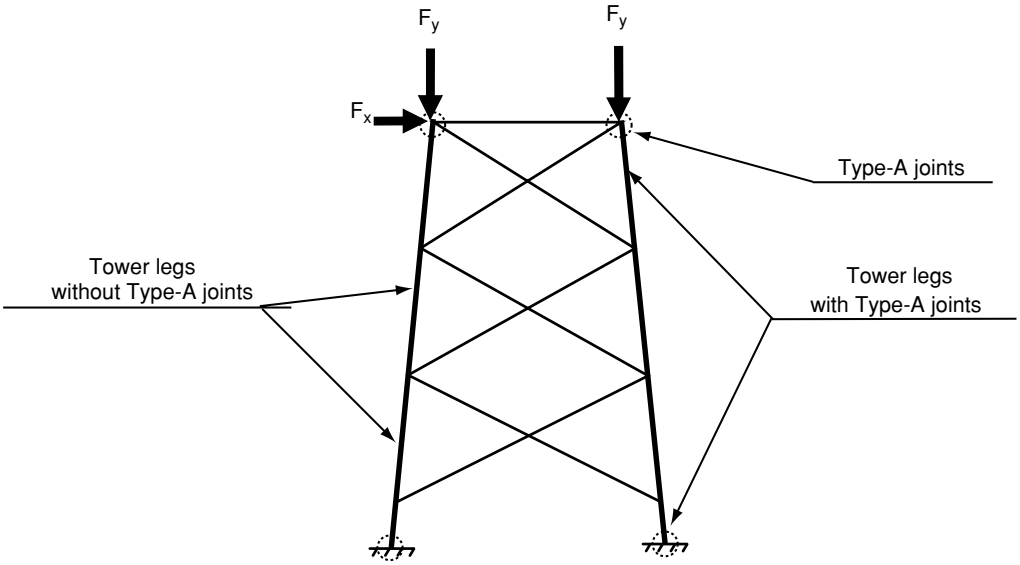

Figure 11. Finite element model of 2-D tower substructure

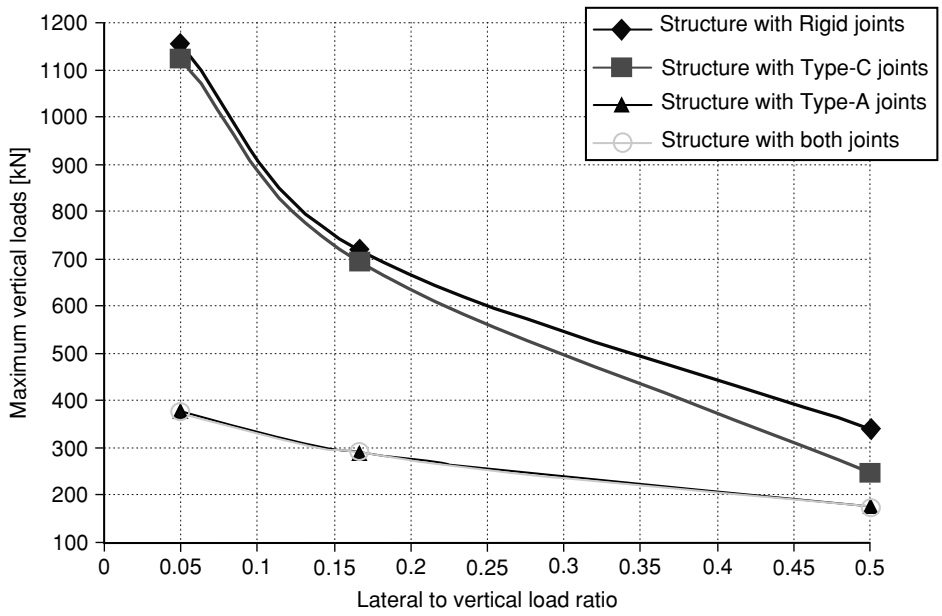

Figure 12. Effect of the Joint Slippage on the Load Carrying Capacity for various test load cases

Type-A joints is considered, the load-carrying capacity is less than one-half the capacity of a structure with ideal joints. Similar results occur when all joints have slippage. It is therefore important to note that slippage of tower leg joints can significantly affect the load-carrying capacity of a tower. For the other load cases, Figure 12 also shows that a reduction in the ratio of the lateral-to-vertical loads decreases the effect of the slippage of Type-C joints. In a similar way, increasing this ratio would significantly decrease the load carrying-capacity of the structure.

Figure 13 shows the tip deflections of the structure in the vertical and horizontal directions for various vertical load magnitudes and lateral-to-vertical load ratios. As expected, a structure with ideal joints shows the highest stiffness and therefore the lowest deflections. The presence of joint slippage generally makes a structure more flexible. Slippage of the Type-C joints has more influence on the lateral deflections compared with the Type-A joints. This is probably because Type-C joints connect the diagonal and horizontal bracing members, which have more influence on the overall lateral stiffness than the tower

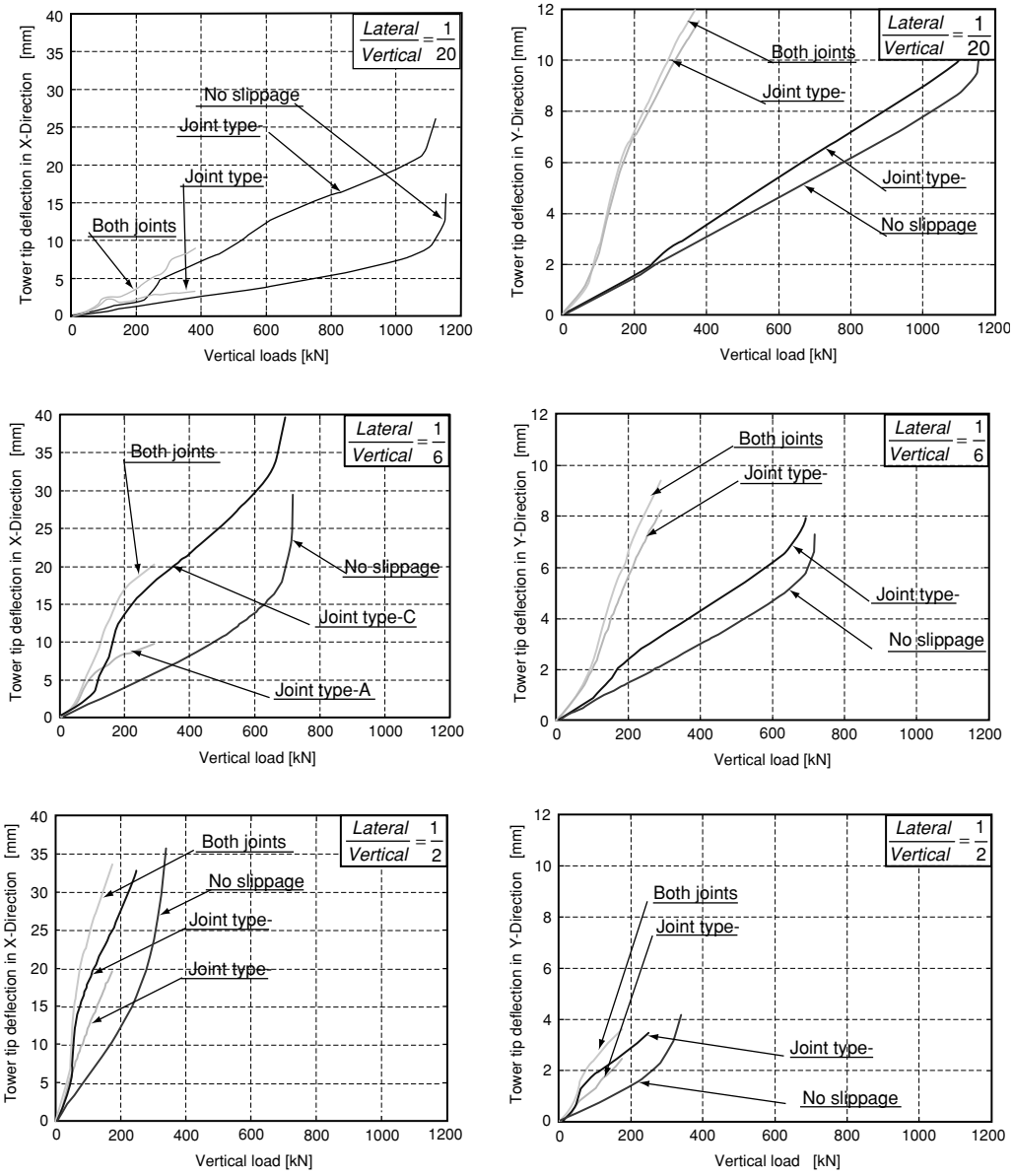

Figure 13. Tower tip deflections in x and y directions for different joint considerations

Table 1. Comparison of yield loads

	Rigid Structure	Structure with Type-A joint	Structure with Type-C joint
Yield Load [kN]	425.0	200.0	75.0

legs do. Similarly, slippage of Type-A joints has more influence on the vertical flexibility of the structure and hence results in higher vertical deflections compared to a structure with rigid joints.

4.2. 3-D Full Scale Tower

A full-scale transmission tower is shown in Figure 14. The tower has 708 angle members with 16 different angle sizes from L51 × L51 × 4.8mm in the upper section of the tower to L152 × L152 × 13mm in the bottom section of the tower. The tower is modeled using 500 elements and 217 nodes (Kroeker 2000; Yue 1994). The weight of the neglected secondary members is assumed to be 20% of the weight of the reduced tower structure (Kroeker 2000; Yue 1994). The tower-leg and horizontal bracing members are modeled as 3-D beam elements. The tower legs elements have a common third node located at the tower center line. The third nodes of the horizontal bracing elements are defined by the

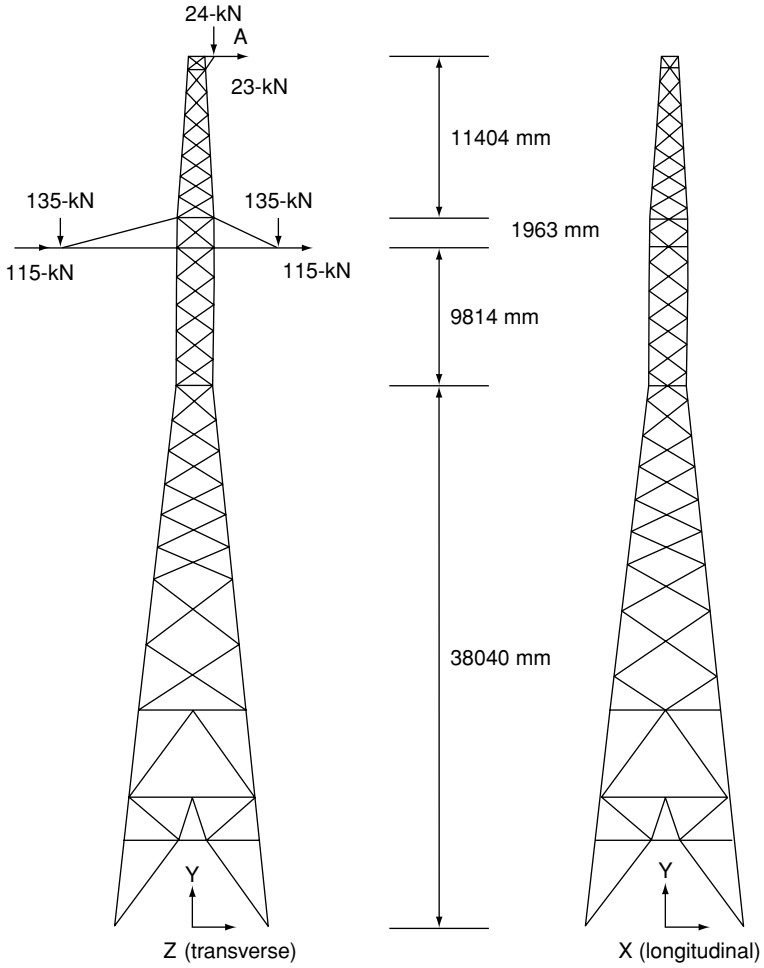

Figure 14. Full-scale transmission tower

Table 2. Comparison of tower deflections at point A

	U_X (mm)	U_Y (mm)	U_Z (mm)
Kroeker (2000)	–0.00	–29.972	531.56
Current Model	0.20577E-14	–33.597	517.29

intersection of the tower center line and the maximum moment of inertia plane of each element. The cross-bracing members are modeled as 3-D truss elements. The loading case shown in Figure 14 is one of the extreme load cases considered by Kroeker (2000).

Table 2 shows that the deflections of Node A (Figure 14) of the tower, without considering the joint slippage, agree closely with the results obtained by Kroeker (2000) under the tower self-weight and external loading shown in Figure 14. The minor differences in the deflections are probably due to the consideration of geometric stiffness in the present analysis.

Figure 15 shows the finite element model of the full-scale transmission tower with the locations of the Type-A joints. Note that Type-C joints are used at all cross bracings. The effects of joint slip on tower response are investigated for several loading cases. These loading cases investigate, first, the response of the structure under its self-weight and wire loads with no frost heave, then combine different frost-heave patterns with the self-weight of the tower structure and wire loads.

The first case is for the tower under its self-weight and the working loads shown in Figure 14. The axial loads of the column and beam elements at a particular height from the tower base are normalized with respect to their yield loads, and the maximum absolute axial load of this group is identified. These normalized maximum axial loads at various heights are then plotted against the normalized height from the tower base separately for column and beam elements.

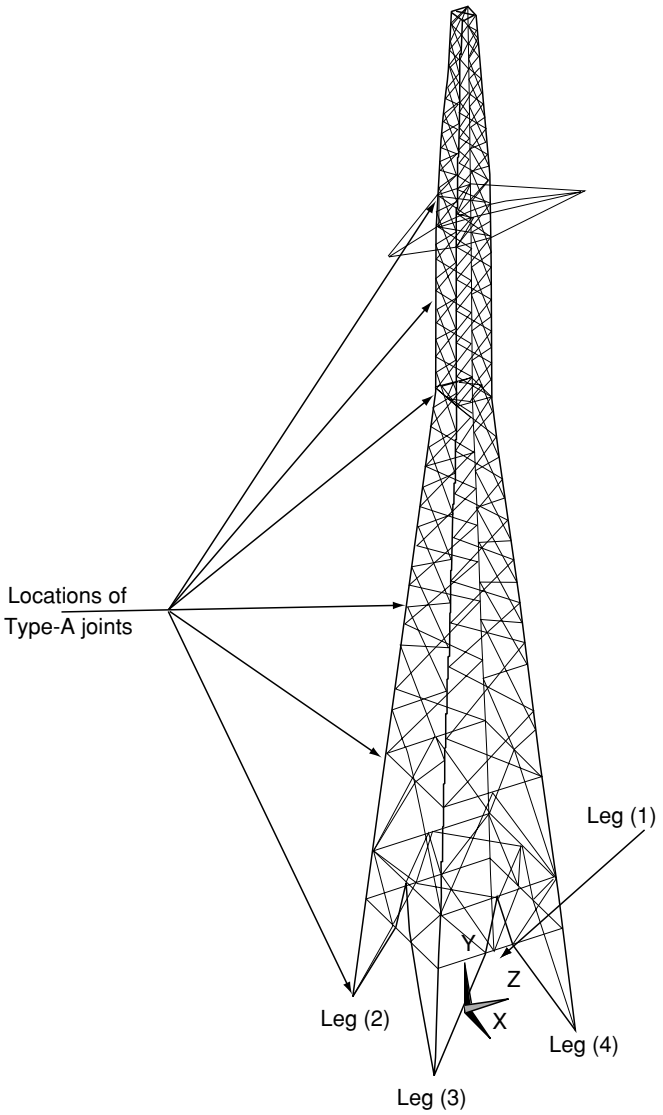

Figure 15. Finite element model of full-scale tower with locations of type-A joints

Figure 16 shows the normalized axial loads of leg members in the presence and absence of joint slippage. Consideration of joint slippage in the analysis results in slightly higher axial loads in the tower legs, as shown in Figure 16. The results for the diagonal and horizontal bracing elements are shown in Figure 17. As expected, the maximum axial loads in the diagonal and horizontal bracing members are generally smaller than that in column members, and a majority of these elements have axial loads less than 30% of the yield load.

Figures 18 and 19 show the normalized axial loads of the tower leg elements due to a frost-heave induced displacement of Leg #2 by 100 mm, without joint slippage. Ignoring joint slippage in the analysis results in significant increases in the member axial loads, and some members near the tower base show loads above their failure loads. Similar behaviour is also noted for the bracing members near the tower base. The corresponding results for a tower with joint slippage are shown in Figures 20 and 21. Consideration of joint slippage in the analysis yields force profiles that are quite similar in shape and magnitude to the case when there is no frost-heave induced displacement. Including joint slippage in the analysis, however, results in member axial force increasing by only 27% maximum at the tower base level, with negligible changes in the axial forces in the top half of the tower. These results confirm that in a real tower, joint slippage contributes to a substantial redistribution of forces when subjected to frost-heave induced displacements. As a result, the maximum axial forces in tower leg members are substantially lower than those corresponding to a tower with ideal joints.

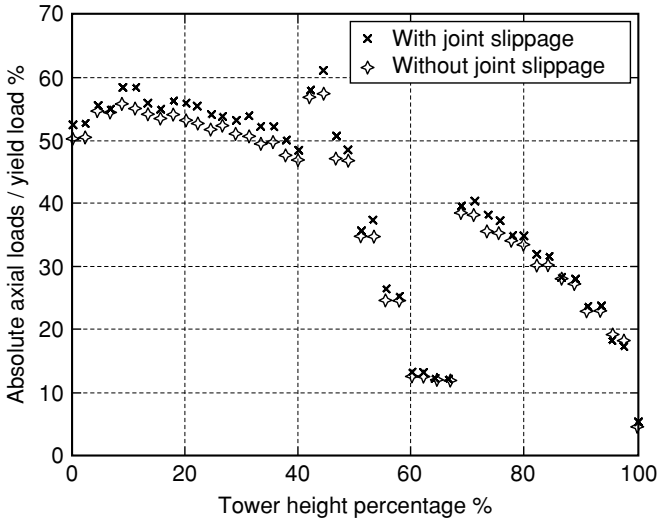

Figure 16. Normalized axial load of tower legs under self-weight and applied loading with and without joint slippage

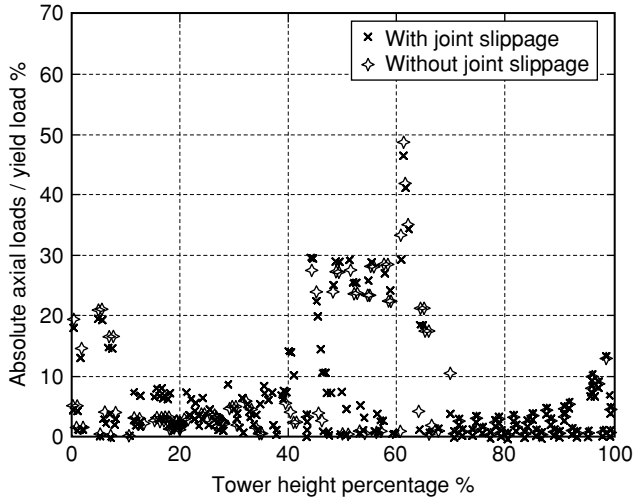

Figure 17. Normalized axial load of diagonal and horizontal bracing members under self-weight and applied loading with and without joint slippage

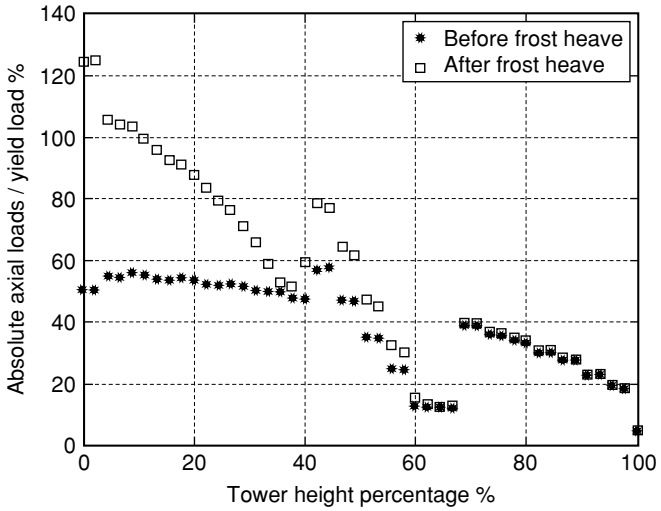

Figure 18. Normalized axial load of tower legs due to a frost-heave induced displacement of 100 mm (without joint slippage)

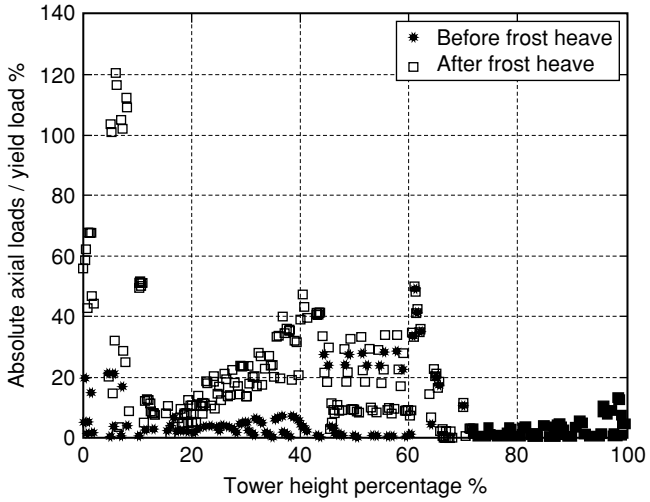

Figure 19. Normalized axial load of diagonal and horizontal bracing members due to a frost-heave induced displacement of 100 mm (without joint slippage)

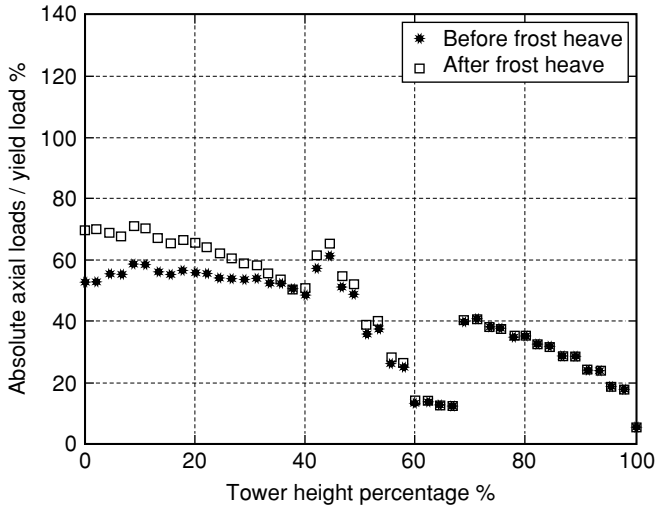

Figure 20. Normalized axial load of tower legs due to a frost-heave induced displacement of 100 mm (with joint slippage)

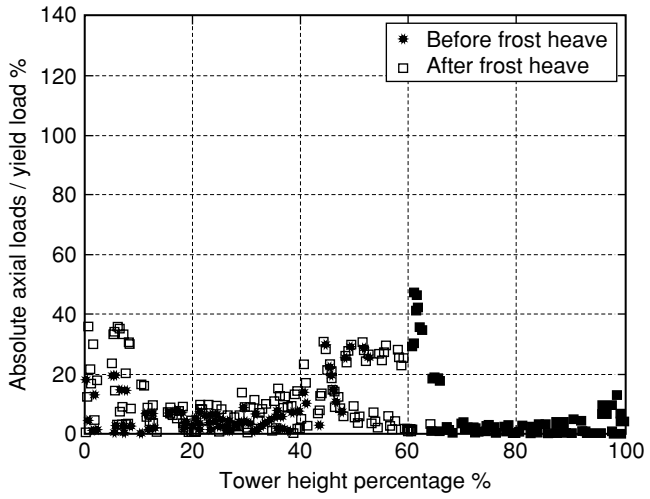

Figure 21. Comparison of normalized axial load of horizontal bracings due to a frost-heave induced displacement of 100 mm (with joint slippage)

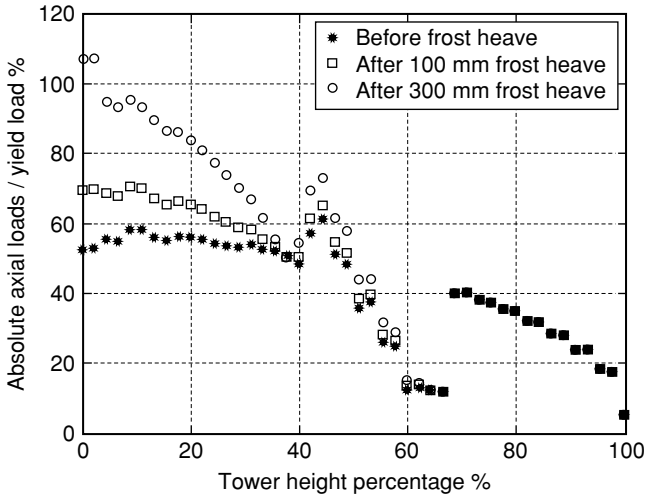

Figure 22. Normalized axial load of tower legs due to different frost heave displacements (with joint slippage)

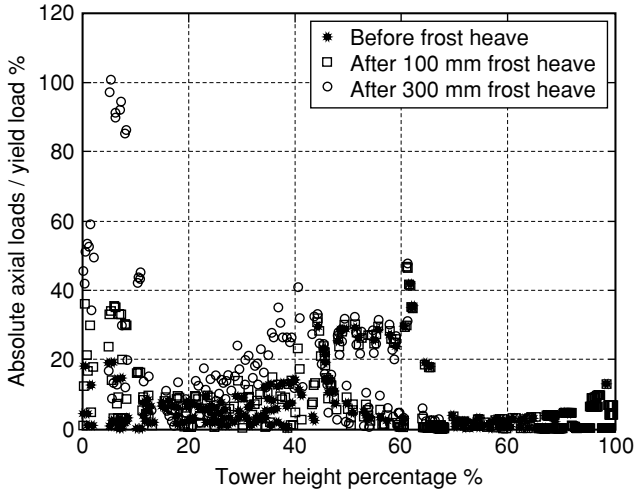

Figure 23. Normalized axial load of horizontal bracings due to different frost heave displacements (with joint slippage)

In the last loading case, a frost-heave displacement of 300 mm is experienced by Leg #2. This loading case can be considered to represent an extreme frost-heave condition observed in northern Manitoba. Although towers subjected to such large frost-heave displacements are found to show no failure in the field, the forces obtained from conventional structural analysis without joint slippage show leg member failure when frost-heave displacements exceed 200 mm. Figures 22 and 23 show that the tower leg member forces are lower than the yield loads when joint slippage is included in the analysis, except in the case of leg members at the tower base. This finding shows that actual tower member forces due to frost-heave are much lower than those predicted by an analysis based on the rigid joint assumption. It is therefore clear that joint slippage has a very positive effect on towers subjected to frost-heave.

5. CONCLUSIONS

In the current work, a finite element model, based on experimentally observed slippage behaviour of bolted joints of transmission towers, is developed to examine the behaviour of towers subjected to various loading, including frost-heave induced displacements. The numerical study shows that slippage of tower leg and bracing member joints has a significant effect on the load-carrying capacity of a transmission tower depending on the ratio of the lateral load to the vertical load. It is found that the effect of slippage of tower leg joints is more significant than that due to bracing member joints. It is also found that slippage of

tower leg joints contributes substantially to vertical deflections of a tower, whereas slippage of tower bracing joints contributes to the lateral deflections.

The analysis of a 3-D full-scale tower shows that joint slippage has a minor influence on tower member forces due to tower self-weight and cable loads. However, the study of the response of a tower under different frost-heave induced displacements shows that upward displacement of a single leg induces large axial forces in tower members if joint slippage is neglected. Frost-heave induced displacement of two adjacent tower legs, however, causes minor changes in the tower member axial forces. The numerical results show that ignoring joint slippage in the analysis results in tower leg axial forces that are almost twice as high as these corresponding to the case accounts for joint slippage under frost-heave. In the case of bracing elements, the axial forces corresponding to the rigid joint assumption could be as high as six times the forces corresponding to the slippage case. These findings provide a satisfactory explanation of the field observations of towers subjected to frost-heave induced displacements in northern Manitoba. The results also confirm the importance of incorporating bolted-joint slippage in the analysis and design of towers.

ACKNOWLEDGEMENTS

The work presented in this paper was supported by a collaborative research grant from the Natural Sciences and Engineering Research Council of Canada and Manitoba Hydro. The authors acknowledge helpful discussions with Mr. Ben Yue, P.Eng. of Manitoba Hydro.

REFERENCES

Al-Bermani, F.G.A., Kitipornchai, S. and Chan, S.L. (1992). "Formex formulation of transmission tower structures", *International Journal of Space Structures*, Vol. 7, No. 1, pp. 1–10.

Bahaari, M.R. and Sherbourne, A.N. (1996). "3D simulation of bolted connections to unstiffened columns-II. extended endplate connections", *Journal of Construction Steel Reserach*, Vol. 40, No. 3, pp. 189–223.

Calado, L., Mele, E. and De Luca, A. (1999). "Experimental investigation on the cyclic behavior of welded beam-to-column connections", *Proceedings of the 2nd EuropeanConference on Steel Structures*, PRAHA, Czech Republic, Paper No. 215.

Chen, W. and Lui, E. (1987). "Effects of joint flexibility on the behavior of steel frames", *Computers and Structures*, Vol. 26, No. 5, pp. 719–732.

Delvecchio, J.N. and Soom, A. (1991). "Tolerances and available relative motion in bolted connections", *Advances in Design Automation*, ASME, Vol. 2, pp. 177–183.

Ghali, A. and Neville, A.M. (1978). *Structural Analysis – A Unified Classical and Matrix Approach*, Chapman and Hall, London, UK.

Gilchrist, R.T. and Chong, K.P. (1979). "Thin light-gage bolted connections without washers", *Journal of the Structural Division*, ASCE, Vol. 105, No. 1, pp. 175–183.

Kitipornchai, S., Al-Bermani, F.G.A. and Peyrot, A.H. (1994). "Effect of bolt slippage on ultimate behavior of lattice structures", *Journal of Structural Engineering*, ASCE, Vol. 120, No. 8, pp. 2281–2287.

Kroeker, D. (2000). *Structural Analysis of Lattice Towers with Joint Slippage*, MSc. Thesis, The University of Manitoba, Winnipeg, Canada.

Marjerrision, M. (1968). "Electric transmission tower design", *Journal of the Power Division*, ASCE, Vol. 94, No.1, pp. 1–23.

Pai, N.G. and Hess, D.P. (2002). "Three-dimensional finite element analysis of threaded fastener loosening due to dynamic shear load", *Engineering Failure Analysis*, Vol. 9, No. 4, pp. 383–402.

Petersen, W. (1962). "Design of EHV steel tower transmission lines", *Journal of the Power Division,* ASCE, Vol. 88, No. 1, pp. 39–65.

Przemieniecki, J.S. (1968). *Theory of Matrix Structural Analysis*, McGraw-Hill, New York, USA.

Ungkurapinan, N., Chandrakeerthi, R., Rajapakse, R.K.N.D. and Yue, B. (2003). "Joint slip in electrical transmission towers", *Engineering Structures*, Vol. 25, No. 6, pp. 779–788.

Ungkurapinan, N. (2000). *A Study of Joint Slip in Galvanized Bolted Angle Connections*, MSc. Thesis, University of Manitoba, Winnipeg, Canada.

Williams, D.C.J. and Brightwell, I.W. (1987). "Stochastic method of assessing the effect of joint deformation on bolted lattice towers", *Proceedings of the 1st International Symposium on Probabilistic Methods Applied to Electric Power Systems*, pp. 365–373.

Winter, G. (1956). "Tests on bolted connections in light gage steel", *Journal of Structural Division*, ASCE, Vol. 82, No. 2, pp. 1–25.

Yue, B. (1994). *Tower Design and Analysis Program User Manual*, Manitoba HydroTransmission and Civil Design Department, Winnipeg, Canada.

Zienkewicz, O.C. and Taylor, R.L. (1989). *The Finite Element Method*, 4th Edition, McGraw-Hill, London, UK.